

# The Influence of Saturation on the Surface Structure of Mixed Fatty Acid-on-Water Aerosol: A Molecular Dynamics Study

*Aisling C. Stewart, Martin J. Paterson, Stuart J. Greaves*

Institute of Chemical Sciences, Heriot-Watt University, Edinburgh EH14 4AS, United Kingdom

**Supporting Information**

# Contents

S1 Force Field Selection .....	3
S2 Evaluation of the Equilibration Procedure.....	4
S3 Root Mean Square Deviation.....	5
S4 Curvature Effects .....	6
S5 Monolayer Coverage Tests .....	8
S6 Solid Angle Effects in the Tilt Angle Analysis .....	10
S7 Width of the Slabs.....	12
References .....	14

## S1 Force Field Selection

The choice of an appropriate force field is a key pre-requisite of any molecular dynamics (MD) study, to ensure that the simulations carried out will accurately represent the species of interest. In the present study the OPLS-AA force field was employed,<sup>1</sup> with parameters obtained via the LigParGen server.<sup>2</sup> This selection was based on tests of simulations of bulk samples of each of the acids used at the temperature used in the current work. These simulations were carried out by filling a box of diameters 6.5 x 6.5 x 6.5 nm with 300 molecules of a given acid, carrying out an energy minimization using the steepest decent algorithm and then carrying out NVT and NPT equilibration steps. The NVT equilibration employed a leap-frog algorithm,<sup>3</sup> with a time step of 0.5 fs and a length of 50 ps. The NPT equilibration was carried out in two steps. This first used a leap-frog algorithm combined with a modified Berendsen thermostat for 5 ns.<sup>4</sup> The second used a velocity Verlet algorithm<sup>5</sup> and Martyna-Tuckerman-Tobias-Klein (MTTK) pressure coupling,<sup>6</sup> also lasting 5 ns for the oleic acid samples and 10 ns for the stearic acid samples, which required longer to reach equilibrium. Analysis was carried out on the last 4 ns of these MTTK steps in order to obtain the densities and viscosities of the acid samples for each of the force fields tested. The results of these studies are shown in Table S1. The force fields tested were the OPLS-AA,<sup>1</sup> Gromos54a7<sup>7</sup> and Generalised AMBER Force Field (GAFF).<sup>8</sup>

Density/g mL <sup>-1</sup>								
	Experimental (Literature)	Calculated			% Difference			
		OPLS-AA	Gromos54a7	GAFF	OPLS-AA	Gromos54a7	GAFF	
Oleic Acid (298 K) <sup>9</sup>	0.89	0.89±0.00	0.91±0.00	0.86±0.00	0.0	2.3	-3.4	
Stearic Acid (293 K) <sup>10</sup>	0.94	0.90±0.00	0.98±0.00	0.93±0.00	-4.4	+4.4	-1.1	
Viscosity/Cp								
	Experimental (Literature)	Calculated			% Difference			
		OPLS-AA	Gromos54a7	GAFF	OPLS-AA	Gromos54a7	GAFF	
Oleic Acid (293 K) <sup>11</sup>	34.82	133.15±1.68	22.17±0.14	8.78±0.07	+282.84	-36.32	-74.8	
Oleic Acid (303 K) <sup>11</sup>	15.92	14.73±0.28	36.26±0.14	42.15±0.24	-7.475	+127.8	+164.8	
Stearic Acid (343 K) <sup>12</sup>	9.87	49.25±0.23	162.86±0.46	65.73±0.16	+399.0	+1550	+566.0	

**Table S1** Selected bulk properties of oleic and stearic acid, as calculated by MD simulations using the Gromos54a7 and GAFF and OPLS-AA force fields, along with literature experimental values. The left-hand columns display the raw values. The right-hand columns show the deviation of the calculated from the experimental quantities (

$$\Delta_{value} = \frac{Simulated\ Value - Experimental\ Value}{Experimental\ Value} \times 100$$

.These are given as a percentage.

## S2 Evaluation of the Equilibration Procedure

The production runs analyzed in the main paper were for the fully equilibrated slabs. This equilibration process was carried out in stages, with shorter energy minimization and NVT steps being implemented as each molecule was added to the slab, followed by a longer NVT equilibration run after all the molecules had been added. The short (50 ps) NVT steps between the addition of molecules were intended to ensure that the molecules had a chance to find the slab before new molecules were added, in order to avoid the formation of large droplets of organic molecules away from the main slab. These steps were not intended to fully equilibrate the slab.

The longer equilibration step lasted 10 ns. This time was chosen based on partial density and SASA analysis on simulations that had been carried out for different lengths of time. There was found to be no significant change in the results of these analysis procedures on increasing the simulation length from 10 ns to 30 ns and it was therefore concluded that 10 ns was sufficient for generating a fully equilibrated slab. This was investigated by running an equilibration step that lasted a total of 30 ns, dividing the resulting trajectory into 5 ns long fragments and carrying out SASA and partial density analysis across each of the fragments. An example of this analysis on one composition of slab (a slab containing equal numbers of oleic and stearic acid molecules) is shown below in Fig. S1 and S2. As an additional measure to ensure that the results shown in the main paper were from fully equilibrated slabs, the first 4 ns of the production runs were not included when extracting information from the production runs, in order to give the samples additional time to stabilize at the beginning of each run.

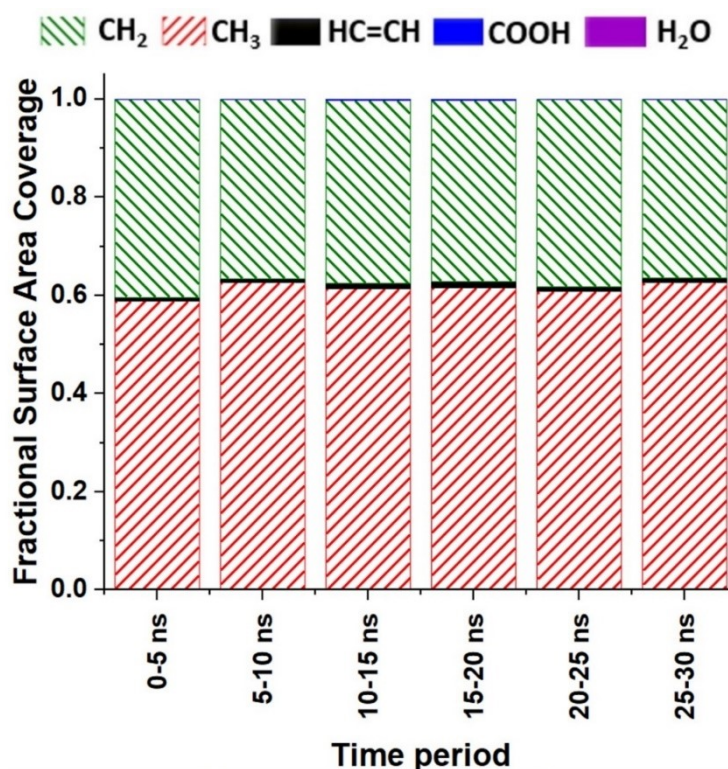


**Fig. S1** SASA coverages for different functional groups for a slab containing equal amounts of stearic and oleic acid. Each bar represents analysis being carried out over a different time interval within the equilibration of this single slab. A probe of radius 0.22 nm has been used and averaging has been carried out over the bottom and top faces of the slab.

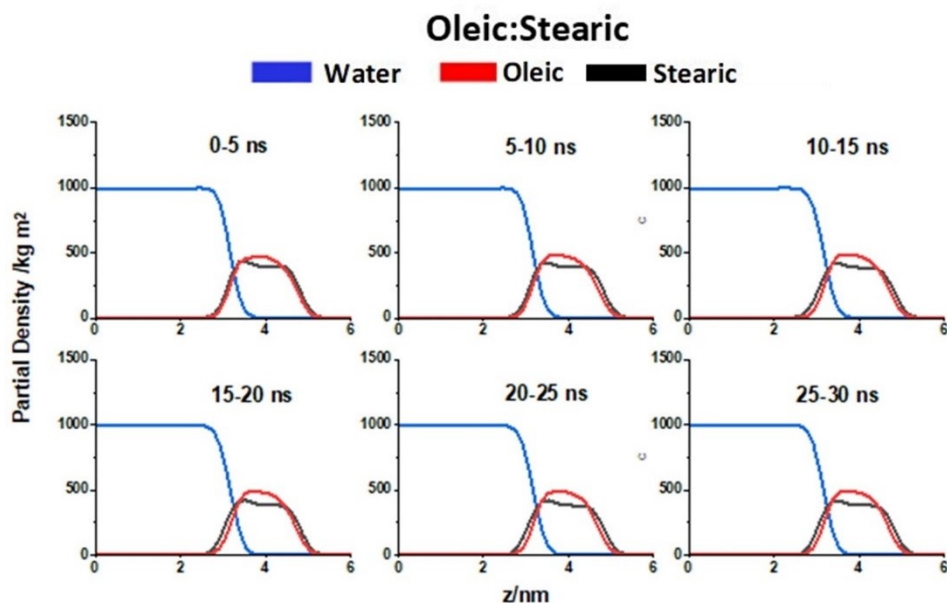


**Fig. S2** Partial density analysis for different species for a slab containing equal amounts of stearic and oleic acid. Each bar represents analysis being carried out over a different time interval within the equilibration of this single slab. The data is an average over the positive and negative  $z$  directions but has not been normalized.

### S3 Root Mean Square Deviation

Another way of obtaining information about the equilibration times of the samples is to study the root mean square deviation (RMSD) of the trajectories. This is a measurement of the deviations of the atoms from their positions at a reference point, here those at the start of the run, and it can be calculated as part of the GROMACS software package. Example RMSD calculations are shown below (Fig. S3). The calculation has been carried out for three different compositions of slab – a slab containing only stearic acid in its organic layer, one containing only oleic acid and one containing equal amounts of both. The RMSD values were calculated every 5 ps over the 10 ns runs. It can be seen that the RMSD values rapidly reach a plateau, well within the 4 ns that are excluded from the analysis used to extract the data for the main paper (see Section S2). This again supports our decision to use times 4-10 ns of the production run for obtaining information about the equilibrium properties of the slab. The slab containing only oleic acid in its organic layer reaches a plateau more rapidly than the other

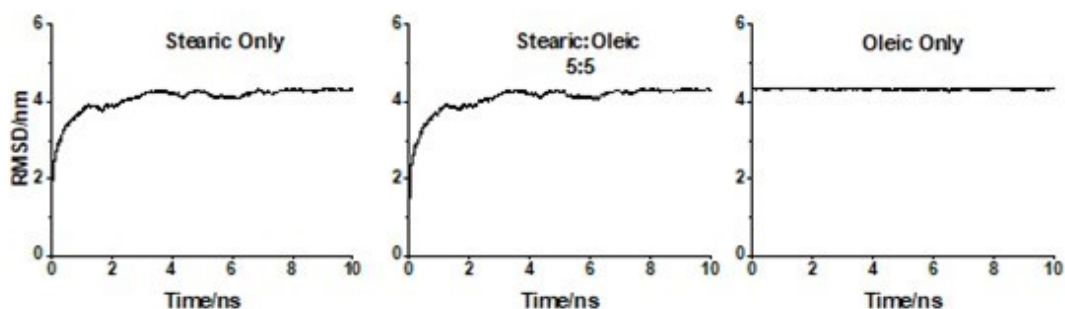


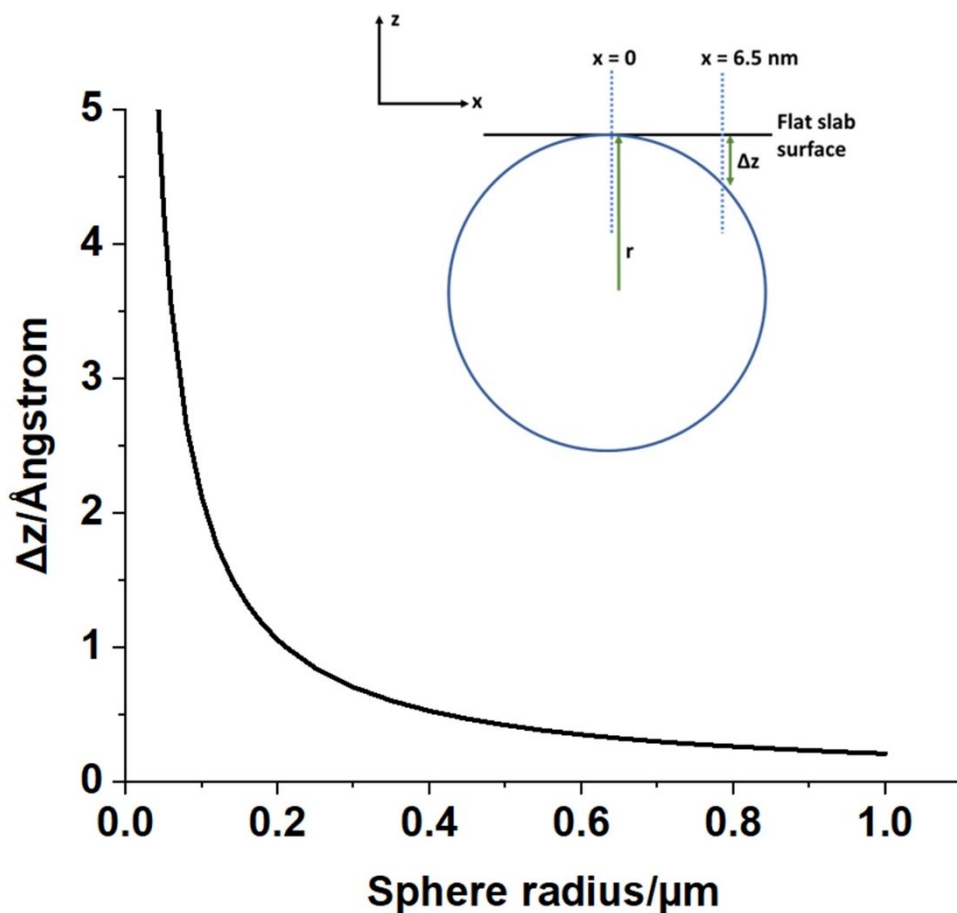
**Fig. S3** RMSD plots for three different compositions of slab, with values calculated every 5 ps over the 10 ns production runs. The plots each reach a plateau rapidly, suggesting that the slabs are well equilibrated.

two slabs. This is likely due to its chains being less tightly packed and therefore more easily able to move past each other and reach equilibration more rapidly.

## S4 Curvature Effects

The calculations employed in this study to investigate the water-organic interface of an aerosol use a flat slab to mimic a portion of the surface of this aerosol particle. The slab is of infinite length in the x and y directions. The z direction consists of a water slab in the center, with acid molecules attached to the upper and lower surfaces of this and areas of vacuum above and below these regions. This is achieved using periodic boundary conditions and a simulation of dimensions  $x = 6.5$  nm,  $y = 6.5$  nm and  $z = 15$  nm, which is repeated indefinitely in all directions. Aerosols, however, are droplets and therefore have a certain degree of curvature, which could affect the properties of their surface layer, as compared to a flat sample.

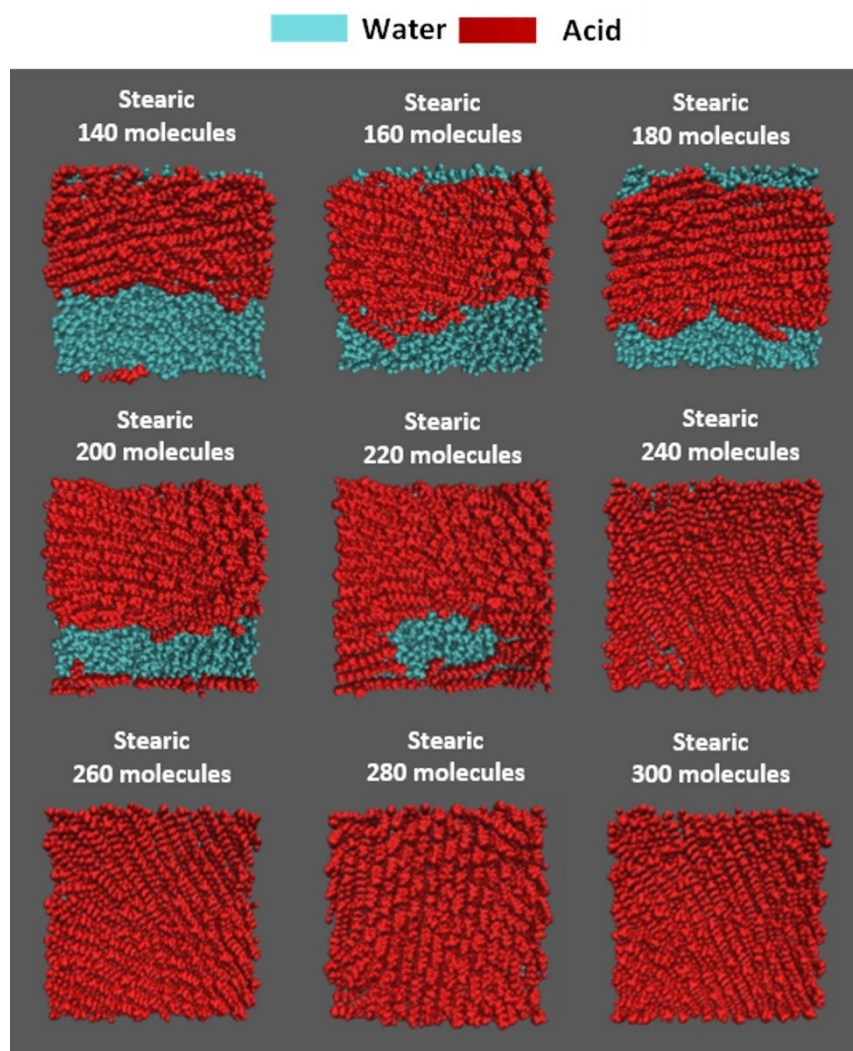
In order to investigate the possible significance of this curvature, it was assumed that a cut-through of an aerosol of radius  $r$  could be described in 2D as circle of the same radius. A portion of the surface of the aerosol is then described as an arc along this circle. Assuming that this arc starts at the one edge of the periodic box in the x dimension ( $x_0$ ) and ends at the other edge ( $x_f = x_0 + 6.5$  nm) the change in z ( $\Delta z$ ) on the surface of the circle between  $x_0$  and  $x_f$  can be calculated (see Fig. S1, insert). The graph in Fig. S1 shows how  $\Delta z$  varies for  $x_f - x_0 = 6.5$  nm (the length of our simulation box) for circles of different radii. For a flat surface, however, this change would be, by definition, zero. It can be seen that for aerosols of radii above  $0.21$   $\mu\text{m}$  the deviation is less than one Ångstrom. One Ångstrom is less than a typical bond length within organic species and it can be seen from the side-on view of the slab in Fig 2 of the main paper and the  $\Delta z$  density plots in Fig. S6 that the typical surface roughness is significantly greater than  $1$  Å. Therefore, a flat sample is a good approximation to a curved one for radii of these values. Aerosol particles of radii  $>0.21$   $\mu\text{m}$  include those within the accumulation mode of aerosol growth and account for a large proportion of the aerosol mass and surface area within the atmosphere.<sup>13</sup> Indeed, flat slabs have been used previously in a few studies to investigate the structure of aerosol surfaces.<sup>14,15</sup>



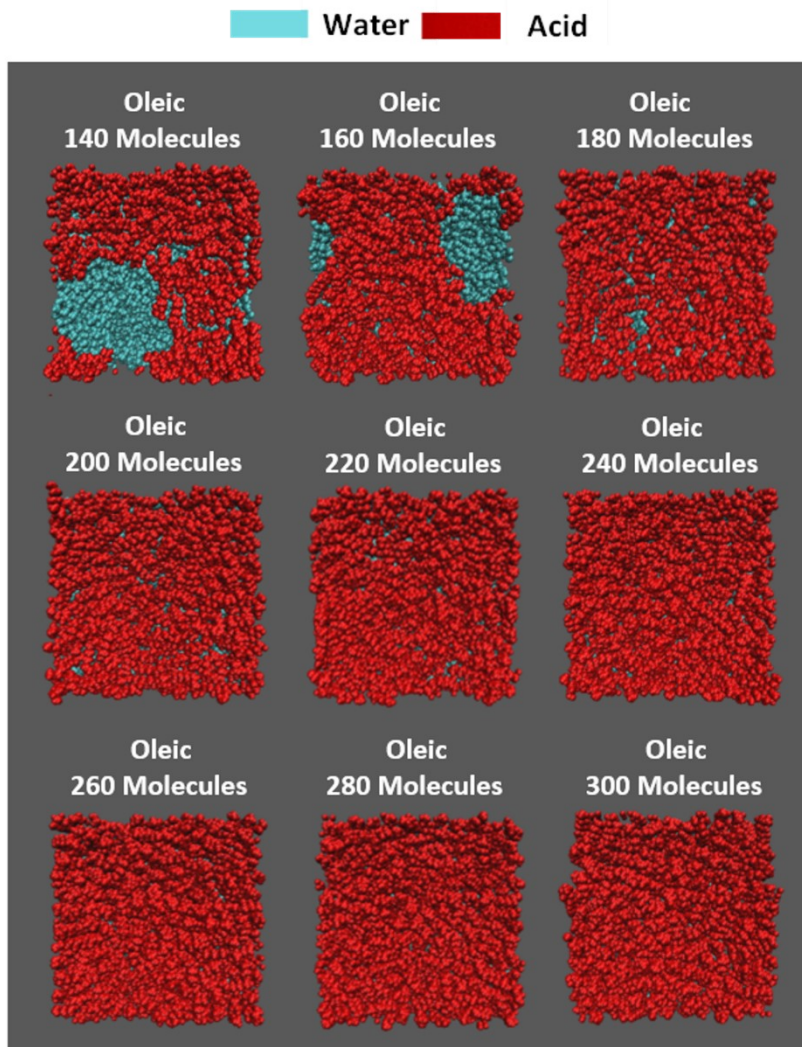
**Fig. S4** How the deviation of the  $z$  coordinates of a sphere differ, at  $x=6.5 \text{ nm}$ , from those of a tangent to it, with this tangent meeting the sphere at  $x=0$ . For spheres of radius  $>0.21 \mu\text{m}$  it can be seen that this deviation is below one Ångstrom and is well below deviations in surface position caused by atomic level roughness. Inset: diagram defining the main parameters discussed above. Aerosols are often modelled as spheres of radius  $r$ . A flat surface represents a tangent to this sphere, meeting at point  $x=0$ . At  $x=0$  the surface of the sphere now has  $z$  coordinates that differ from those of the flat surface by  $\Delta z$ . If  $\Delta z$  is significantly more than the atomic level surface roughness then then curvature effects are considered to be significant over the length of one periodic box.

## S5 Monolayer Coverage Tests

The work reported in this paper was based around a monolayer of fatty acid molecules on a water slab. In order to achieve this, monolayer fatty acid molecules were added at random, to a periodic box of dimensions 6.5 x 6.5 x 15 nm, containing a central water sample of dimensions 6.5 x 6.5 x 6.5 nm. To estimate the number of fatty acids required to achieve an approximately monolayer coverage, a series of test simulations were carried out, adding differing numbers of oleic or stearic acid molecules to the periodic box, in the same manner as described in the Methods section of the main paper, before equilibrating for 10 ns under NVT conditions. Top-down views of the resulting slabs are shown below (Figures S2 and S3). Water molecules are shown in cyan and acid molecules in red, with each of these displayed using their van der Waals volumes. It can be seen that for slabs below 200-240 organic molecules, water molecules are clearly visible from above, whereas for 260 upwards there these are barely visible, suggesting that there is at least a monolayer coverage of acids for these samples. 260 organic molecules was the number chosen to represent a monolayer coverage for the work discussed in the main text.



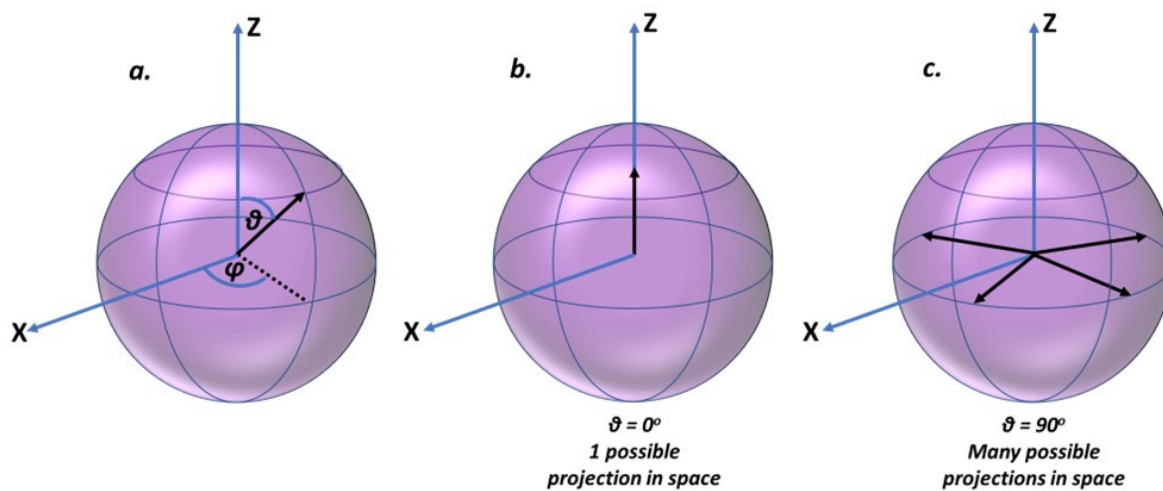
**Fig. S5** Top-down views of slabs of stearic acid, for each of the surface area coverages studied. Acid molecules are shown in red and water molecules in blue. Views are from the final frame of a 10 ns production run. Atoms are shown using their van der Waals volumes.



**Fig. S6** Top-down views of slabs of oleic acid, for each of the surface area coverages studied. Acid molecules are shown in red and water molecules in blue. Views are from the final frame of a 10 ns production run. Atoms are shown using their van der Waals volumes.

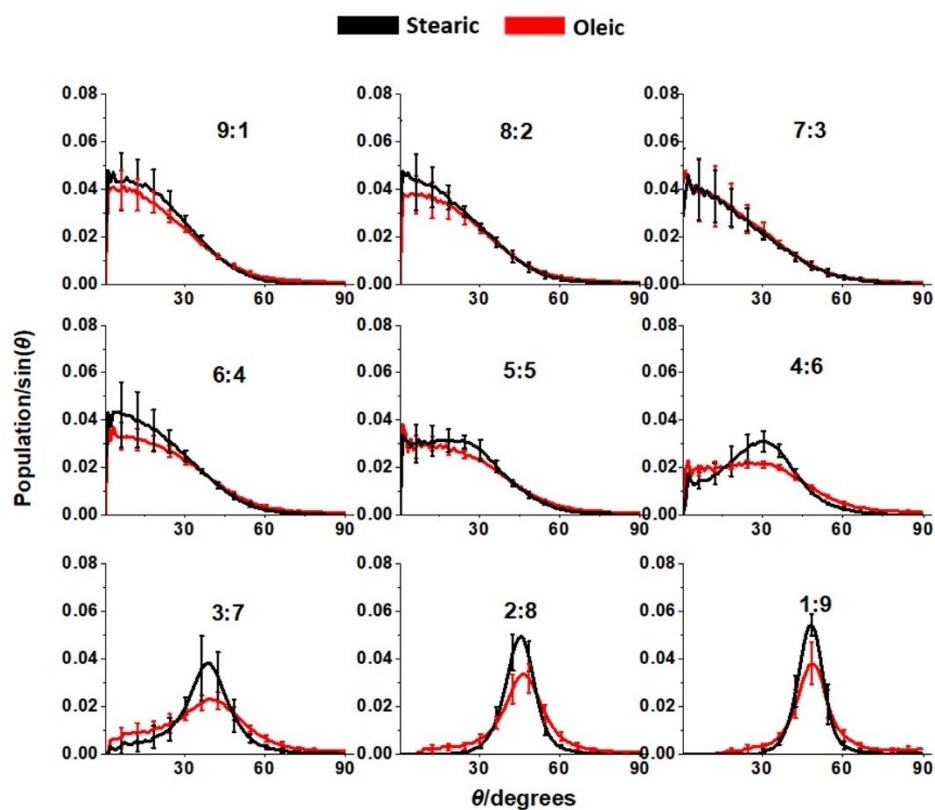
## S6 Solid Angle Effects in the Tilt Angle Analysis

Fig. 7 of the main text shows how the angular distributions of the C1-C18 vectors of the acid molecules with respect to the surface normal are affected by the oleic:stearic ratio of the slabs. However, it should be noted that an isotropic distribution of acid molecules would not give equal distributions across of the angles shown, as the study here only looks at the angle that these vectors make with the z axis (the polar angle,  $\vartheta$ ) and do not take into account the angles that they may make around it (the azimuthal angle,  $\phi$ ). As is shown in Fig. S4 there is only one way in which a vector can be directed and make  $0^\circ$ , whereas there are many ways that they can make  $90^\circ$  to this axis. This solid angle effect can be taken into account by dividing the population at each of value of  $\vartheta$  by  $\sin \vartheta$ , with the results of this being shown Fig. S5 These results further highlight the tendency of molecules to tilt away from the surface normal at higher stearic acid ratios, supporting the arguments made in the main paper.



**Fig. S7** Pictorial depiction of how the solid angle effect influences the populations of different tilt angles. a. Definition of the polar or 'tilt' angle,  $\vartheta$ , referred to in the main paper and the azimuthal angle,  $\phi$ . b. For angles  $\vartheta = 0^\circ$  there is only one possible projection of a vector onto the equatorial plane (zero projection). As theta increases so does the number of projections onto this plane up to a maximum at  $\vartheta = 90^\circ$  (c.). This effect can be taken into account by dividing the angular populations by  $\sin(\vartheta)$  (see Fig. S5).





**Fig. S8** The results of dividing the angular populations from Fig. 7 of the main text by  $\sin(\theta)$ , in order to take into account the solid angle effects discussed above. The error bars represent the error values from Fig. 7 (one standard error of the mean) divided by  $\sin(\theta)$ . The results shown in this figure highlight the shift of the tilt angles of molecules towards higher angles with increasing stearic acid component.

## S7 Width of the Slabs

In this study the water-organic interface of aerosols is mimicked using a slab of water that has organic molecules attached to both the bottom and the top of it. The fact that both sides of the slab are used allows for averaging over twice as many water-organic interactions, thus effectively doubling the sample size with only a small increase in computational cost. However, it is important that the water layer is thick enough that organic molecules cannot interact with each other through it. For the work described in this paper a 6.5 x 6.5 x 6.5 nm box of water was used as the starting point for the aerosol core. This box was then expanded to 15 nm in the z direction, so that areas of vacuum formed above and below the slab, to which the organic molecules were then added.

To investigate whether the thickness of the water core was sufficient for the top and bottom interfaces of the slab to be independent of each other a test simulation was carried out with an initial water core that was twice as thick. Density analysis was carried out on key functional groups to see whether the distributions of these were impacted by the differing thicknesses of water core. Here two slabs have been created by generating boxes of water molecules using the SPC/E model of water. 260 oleic acid molecules were added one by one to each of these boxes, as per the procedure in the Methods section of the main paper. The resulting slabs were then equilibrated under NVT conditions for 10 ns at 298.15 K, as for the other simulations. Analysis was carried out using the gmx density function of GROMACS. This splits the simulation into 100 slices in the z direction and calculates the densities of selected functional groups in each of these slices.

The results are shown in Fig. S6, the upper panel represents the usual 6.5 x 6.5 x 6.5 nm water core (8925 water molecules), expanded into a box otherwise filled with vacuum, with final dimensions 6.5 x 6.5 x 15 nm. For the lower panel the core is 6.5 x 6.5 x 13 nm (17919 water molecules), with a final box side of 6.5 x 6.5 x 21.5 nm, so that the total volumes of the vacuum above and below the water core was the same for each sample. Density analysis was averaged over the top and bottom surfaces of the slab, with the center of the slab set to  $z = 0$ . The results have also been normalized so that the total area under the curve is the same for each of the functional groups.

It can be seen from the two panels that, although the water naturally extends to higher values of z for the slab with more water molecules in it there is no significant difference in the distributions of the functional groups relative to the edge of the water densities. This suggests that the ordering of the molecules is only dependent on the presence of the water and those molecules that are on the same side of the slab as it, and not those on the opposite side. In addition to that the fact that the water density plateaus to a set density for a significant distance in each of the slabs suggests that it has reached its bulk density at the center of the slab and that there is a region of the water core which is not being affected by the presence of the organic molecules on either surface. Both these observations demonstrate that the thickness of the water core chosen for the calculations used in the main text is sufficient for the two sides of the slab to be independent of each other.

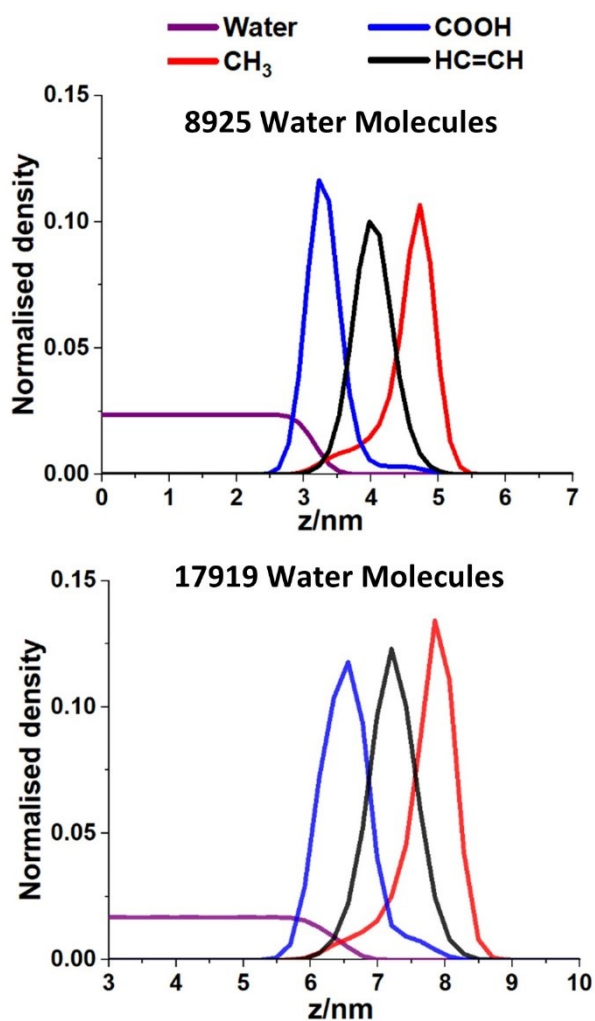


**Fig. S9** Partial density analysis for two slabs, both containing 260 oleic acid molecules but with differing numbers of water molecules at the slab core. The upper plot contains the same number of water molecules as used in the calculations discussed in the main paper, with the lower plot containing twice as many water molecules. The distributions of several key functional groups are shown, relative to the center of the slab ( $z = 0$ ). Each curve is the average of results at time  $> 4$  ns from a 10 ns production runs. Each of the curves has been area normalized to 0.5, accounting for the different numbers of each of the functional groups present within the samples. The curves are each averages over the top and bottom of the slab. The x scale has been adjusted for easier comparison so that the peaks align, but the scale spacing is the same for both plots.

## References

1. W. L. Jorgensen, D. S. Maxwell, J. Tirado-Rives, Development and Testing of the OPLS All-Atom Force Field on Conformational Energetics and Properties of Organic Liquids, *J. Am. Chem. Soc.*, 1996, 118, 11225–11236.
2. L. S. Dodda, I. C. De Vaca, J. Tirado-Rives, W. L. Jorgensen, LigParGen Web Server: An Automatic OPLS-AA Parameter Generator for Organic Ligands, *Nucleic Acids Res.*, 2017, 45, W331–W336.
3. R.W. Hockney, S.P. Goel, and J. Eastwood, Quiet High Resolution Computer Models of a Plasma, *J. Comp. Phys.*, 1974, 14 148–158.
4. H.J.C. Berendsen, J.P.M. Postma, A. DiNola, and J.R. Haak, Molecular Dynamics with Coupling to an External Bath, *J. Chem. Phys.*, 1984, 81, 3684–3690.
5. W.C. Swope, H.C. Andersen, P.H. Berens, and K.R. Wilson, A Computer-Simulation Method for the Calculation of Equilibrium-Constants for the Formation of Physical Clusters of Molecules: Application to Small Water Clusters, *J. Chem. Phys.*, 1982, 76, 637–649.
6. G. J. Martyna, D. J. Tobias, M. L. Klein, Constant Pressure Molecular Dynamics Algorithms, *J. Chem. Phys.*, 1994, 101, 4177–4189.
7. N. Schmid, A. P. Eichenberger, A. Choutko, S. Riniker, M. Winger, A. E. Mark, W. F. Van Gunsteren, Definition and Testing of the GROMOS Force-Field Versions 54A7 and 54B7, *Eur. Biophys. J.*, 2011, 40, 843–856.
8. J. Wang, R. M. Wolf, J. W. Caldwell, P. A. Kollman, D. A. Case, Development and Testing of a General Amber Force Field, *J. Comput. Chem.*, 2004, 25, 1157–1174.
9. D. Sagdeev, I. Gabitov, C. Isyanov, V. Khairutdinov, M. Farakhov, Z. Zaripov, I. Abdulagatov, Densities and Viscosities of Oleic Acid at Atmospheric Pressure, *J. Am. Oil Chem. Soc.* 2019, 96, 647–662.
10. D. R. Lide, in *CRC Handbook of Chemistry and Physics*, CRC Press, Boca Ranton, Florida, 95<sup>th</sup> ed., 2014.
11. H. Nouredini, B. C. Teoh, L. D. Clements, Densities of Vegetable Oils and Fatty Acids, *J. Am. Oil Chem. Soc.*, 1992, 69, 1184–1188.
12. M. O. Bagby, in *Kirk-Othmer Encyclopedia of Chemical Technology*, John Wiley & Sons, New York, 1999.
13. T. Zhang, Z. Zhu, W. Gong, H. Xiang, R. Fang, Characteristics of Fine Particles in an Urban Atmosphere - Relationships with Meteorological Parameters and Trace Gases, *Int. J. Environ. Res. Public Health*, 2016, 13, 807(1-16).
14. O. Ozgurel, D. DufLOT, M. Masella, F. Réal, and C. Toubin, A Molecular Scale Investigation of Organic/Inorganic Ion Selectivity at the Air-Liquid Interface, *ACS, Earth and Space Chemistry*, 2022, 6, 1698-1716.
15. S. Takahama and L. M. Russell, A Molecular Dynamics Study of Water Mass Accommodation on Condensed Phase Water Coated by Fatty Acid Monolayers, *Aerosol and Clouds*, 2011,116, D02203(1-14).

